Geopersia 2021, 11(1): 115-130
DOI: 10.22059/GEOPE.2020.296123.648526

RESEARCH PAPER

Detection of rare earth element anomalies in Esfordi phosphate deposit of Central Iran, using geostatistical-fractal simulation

Mojtaba Shamseddin Meigoon[1], Mohammad Lotfi [2,*], Peyman Afzal [3], Nima Nezafati [1], Maryam Kargar Razi [4]

[1] Department of Earth Sciences, Science and Research Branch, Islamic Azad University, Tehran, Iran
[2] Department of Geology, North Tehran Branch, Islamic Azad University, Tehran, Iran
[3] Department of Petroleum and Mining Engineering, South Tehran Branch, Islamic Azad University, Tehran, Iran
[4] Department of Chemistry, North Tehran Branch, Islamic Azad University, Tehran, Iran

Received: 05 February 2020, Revised: 14 July 2020, Accepted: 17 August 2020

Abstract
This study is aimed to determine geochemical anomalies of rare earth elements (REEs) and provides a concentration distribution map for the Esfordi phosphate deposit (EPD), Bafq metallogenic province (BMP), Central Iran. With an average grade of 5519 ppm for REEs, the EPD is one of the prominent deposits of the region. In this research, sequential Gaussian simulation (SGS) and concentration-area (C-A) fractal modeling are used to determine concentration anomalies and provide a ∑REEs concentration map based on surface data. The log-ratio matrix is used to investigate the mineralization processes, determining the relationships between the anomalies and the rock units, and validating the results of SGS fractal modeling. The results are indicating that the main anomaly has strong correlation with the apatite-iron, and in particular, with the apatite mineralization, which can be considered as an exploration guide. The results also confirm the efficiency of simultaneous application of fractal modeling and SGS simulation.

Keywords: Sequential Gaussian simulation (SGS), concentration-area fractal modeling, log-ratio matrix, Rare Earth Elements (REEs), Esfordi

Introduction

Different stages of mining always have some degree of uncertainty in parameters such as ore grade and size. The uncertainties that directly affect the technical and economic parameters of exploiting the resources, are sometimes caused by inherent variations of deposits, but in many cases result from limited information imposed by high costs (Kühn & Visser, 2014). To unravel such complicated situations, accurate estimation methods may be an asset. In this regard, determining geochemical anomalies and separating them from the background can be efficiently and precisely used in mineral exploration, geological developments, and in the recognition and interpretation of ore deposits (Cheng et al., 1994; Agterberg, 1995; Wang, 2003; Hassanpour & Afzal, 2013; Afzal et al., 2015; 2016; 2017; Yasrebi & Hezarkhani, 2019; Shahsavar et al., 2020).

To gain a better understanding of the ore deposit situation, it is important to employ methods that take into account spatial distribution of geochemical data. Geostatistics is used to identify and explain the spatial geochemical variability of ore deposits, and ore exploration. The "simple kriging" technique (Journel & Huijbregts, 1978) is one of the most well-known and widely-used methods of geostatistical estimation, but it causes less variability than actual value, and may create statistical uncertainty or even statistical error in non-sampled areas (Emery &

* Corresponding author e-mail: m_lotfi_1014@yahoo.com

Lantuéjoul, 2006; Pardo-Igúzquiza & Atkinson, 2007; Goovaerts, 2008).

Traditional methods, which are often based on interpolation results, do not pay much attention to the uncertainties around the estimated values, and this will be especially effective when data volumes are low. Because awareness of uncertainties is needed in analysis of geochemical anomalies, the possible uncertainties must be calculated and measured in subsequent decisions. Thus, geostatistical simulations can be very worthwhile. They consider concentration distribution as well as local uncertainties (Chen et al., 2012; Madani Esfahani & Asghari, 2013; Soltani et al., 2014; Hajsadeghi et al., 2017). Since in exploratory studies relatively small number of samples are used for a given study area, having different ore-deposit types rather than an average image is important in optimal modeling of anomalies and mineralized zones (Afzal et al., 2014; Hajsadeghi et al., 2017).

Fractal methods (Mandelbrot, 1983) can be considered as one of the most reliable non-Euclidean geometric methods in determining the concentration distribution of an ore in a deposit. These methods, take into account the spatial distribution of the relevant data, and proceed the analysis of the data without distorting it. These methods use data to classify various geological features, especially the separation of anomalies from background. These advantages have led to the widespread usage of fractal methods in geosciences (Davis, 2002; Zuo et al., 2009; Zuo & Xia, 2009; Afzal et al., 2010; 2011; Zuo, 2011a;2011b; Afzal et al., 2012; Carranza et al., 2012; Afzal et al., 2014; Shamseddin Meigoony et al., 2014; Yasrebi, 2014; Afzal et al., 2015; Nazarpour et al., 2015; Afzal et al., 2016; Rezaie & Afzal, 2016; Zuo & Wang, 2016; Afzal et al., 2017; Jebeli et al., 2018; Afzal et al., 2019; Ahmadfaraj et al., 2019; Farahmandfar et al., 2020).

The main objective of the current research is to provide the fractal simulation for total rare elements (∑REEs) using "sequential Gaussian" simulation (SGS) and the "concentration-area" fractal (C-A) method (Cheng et al., 1994) for the Esfordi phosphate deposit located in the Bafq metallogenic province. Moreover, for validation purposes and better understanding of the rock characteristics in the studied deposit, the "log-ratio" matrix proposed by Carranza (2011) is employed.

Methodology

Sequential Gaussian simulation

Geostatistical simulation and its methods are widely used in various branches of geosciences such as exploration and exploitation of natural resources, and environmental studies. Among such methods, the "sequential Gaussian" simulation (SGS) model is the most flexible and practical one (Journel, 1974; Deutsch, 2002; Dubrule, 2003; Asghari et al., 2009; Soltani et al., 2014).

The SGS method assumes the multi-Gaussian nature of the random model function and is based on the logic that the conditional distribution of the observed values can be used to simulate sequential points of the network (Goovaerts, 1997; Asghari et al., 2009). In other words, the algorithm is chosen to simulate a random path that crosses all blocks of the network.

The steps of this method are summarized below (Deutsch & Journel, 1992; Cheuiche Godoy et al., 2001; Queiroz et al., 2001; Soltani et al., 2014):

1) Calculation of the statistical parameters of the initial data and plotting of the relevant histogram;
2) Data normalization;
3) Plotting of a variogram using normal data;
4) Selection of a random path for the simulation;
5) Data estimation on the selected network using one of the kriging methods;
6) Plotting a histogram at any point and random selection of a number from the histogram;

7) Repeating the previous steps for the entire network;
8) Repeating the previous steps for all realizations;
9) Reversing the conversion of the simulated data;
10) Validation.

When SGS simulation is used on a regular network, the method algorithm is usually applied to the central points of each network cell. If the used conditional data is upgraded to a regular network, then the points nominally represent the scale of the network elements. However, if SGS simulation is applied to a series of irregular points, it would be scale difference between the simulated values and the network elements which represent the center points of the unstructured network elements of different shapes and volumes (Asghari *et al.*, 2009; Manchuk, 2010).

C-A fractal model

Cheng *et al.* (1994) developed a "concentration-area" fractal model (C-A) to separate geochemical anomalies from the background. The method employed to describe the relationships between the elemental concentration values and the geological data, based on the amount of area that each specific concentration occupies in the study area; having in mind that by an increase in element concentration, the occupied area decreases (Cheng *et al.*, 1994; Goncalves *et al.*, 2001; Afzal *et al.*, 2010; Daneshvar Saein & Afzal, 2017). This model has the general form of relation 1 (Cheng *et al.*, 1994):

$$A(\rho \leq \vartheta) \infty \rho^{-a_1} ; A(\rho \geq \vartheta) \infty \rho^{-a_2} \quad (1)$$

where $A(\rho \leq \vartheta)$ and $A(\rho \geq \vartheta)$ denote the area with concentration values ρ that are respectively, smaller and greater than contour value ρ defining areas υ, which represents threshold value, and a_1 and a_2 are characteristic exponents for both criteria. The area A (ρ) for a given ρ is equal to the area of cells with grade levels higher than ρ multiplied in the number of cells. The average concentration value is used for cells with more than one sample. Fractures between straight-line segments on the concentration-area log-log plot and the corresponding values of ρ are used as thresholds for separating geochemical values among various components.

Log-ratio matrix

In geochemical and geostatistical studies, after estimation or simulation, the results should be verified and validated. The "log-ratio" matrix (Carranza, 2011) is an efficient tool for checking the compatibility of the two binary models and calculating the accuracy and spatial correlation between them (Table 1).

This method has been used in various exploratory and geological studies, especially in the adaption of geochemical anomalies (both surface and depth) with rock units, alteration zones, and different ore deposit zones (Navidi et al., 2014; Soltani et al., 2014; Carranza, 2017; Jebeli et al., 2018; Gholampour et al., 2019).

Table 1. Log-ratio matrix for correlation between fractal modeling results and geological units

		Geological zone	
		Inside Zone	Outside Zone
Fractal model	Inside Zone	True positive (A)	False positive (B)
	Outside Zone	False negative (C)	True negative (D)
Type 1 error=C/(A+C)		Type 2 error=B/(B+D)	
Overall accuracy= (A+D)/ (A+B+C+D)			

An important parameter in the log-ratio matrix is called overall accuracy (OA), and it is calculated to evaluate the accuracy of anomaly separation from the background, which is the main factor for final decision-making. A higher value of OA indicates a higher correlation. In addition, two types of errors can be calculated using anomalies and background; type 1 error (T1E) indicates the method's capability in background analysis, and type 2 error (T2E) indicates the method's capability in anomaly analysis; lower T2E values are more important than lower T1E ones (Carranza, 2011).

Geological setting

The Esfordi phosphate deposit is located 150 km to the southeast of Yazd and 35 km to the northeast of Bafq. As one of the most important iron and apatite mineralizations in the BMP and Iran, this deposit has a high and significant potential for rare earth elements (Jami et al., 2007; Torab & Lehmann, 2007; Taghipour et al., 2015). The area is a part of the Central Iran zone (Haghipour, 1964; Foerster & Jafarzadeh, 1994; Jami, 2006; Torab & Lehmann, 2007) and Bafq-Poshtbadam subzone (Jami, 2006; Torab & Lehmann, 2007; Taghipour et al., 2015). In terms of metallurgical studies, it lies within the BMP (Figure 1). The Bafq province contains a narrow north-trending rift zone between the Kuhbanan and Kuh Daviran faults. Moreover, it hosts large iron and apatite ore deposits which have formed in nonmetamorphic Early Cambrian rhyolitic to rhyodacitic pyroclastic units (Daliran, 2002; Stosch et al., 2011).

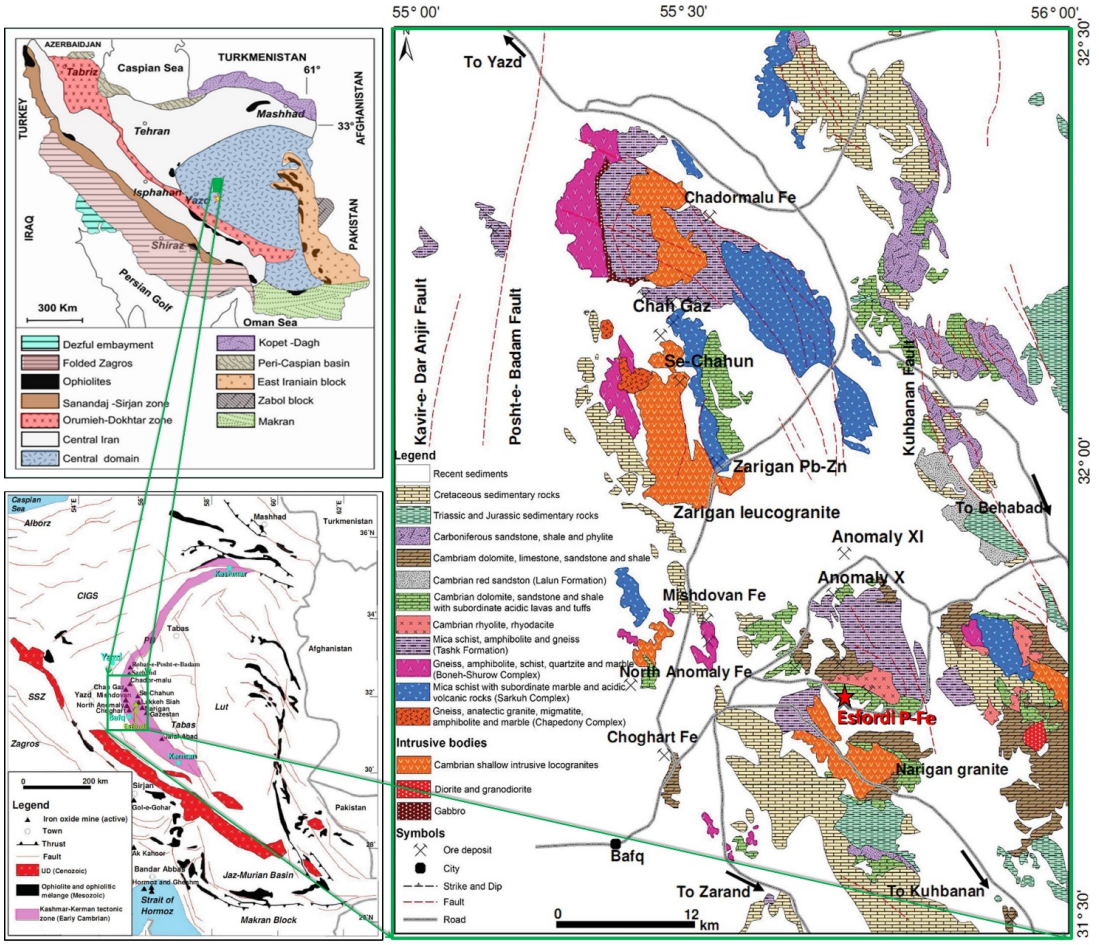

Figure 1. Location of the Esfordi deposit on map of the geological zones of Iran and the geological map of the Bafq metallogenic province (modified after Bonyadi et al., 2011)

The EPD, with an average grades of ~17.2% and ~14% for Fe and P_2O_5 respectively, and having high-grade apatite veins (P_2O_5>35%), is one of the high phosphorus deposits in the region (Torab, 2008). The amount of REE of this deposit, which is LREE-enriched, is close to 2% (Torab & Lehmann, 2007). Apatite crystals are mainly the hosts of REEs in this deposit, but some other host minerals such as monazite, bastnaesite and allanite, are also found as inclusions in apatite (Jami, 2006; Mokhtari, 2015).

The Esfordi deposit forms a U-shaped structure with high altitude in the north, moderate heights in the south and east, and low altitudes in the central and western parts (Figure 2). The general trend of units forming around the northwest-southeast mineral with a westward gradient of 40-50 degrees have been altered by intrusion of igneous rocks and ore-bearing fluids which have created different dips and strikes for the rock layers in each part. As a result of intrusion of igneous masses, a series of fractures followed by disruptions in lithological units have been created. Therefore, this caused the disruption of the primary rock units.

The EPD consists of a series of sedimentary, volcano-sedimentary, intrusive, and extrusive igneous rocks. The adjacent areas and the mining area consist mainly of sedimentary rocks, the oldest rocks in the region, including dolomite and limestone of the Rizu series along with the rhyolite, diabase, syenite, gabbro-diorite, and basalt. Based on the available evidence and studies, the mineralization zones in the mine are of following types (Figures 3 and 4):

Figure 2. Morphological status of the Esfordi deposit

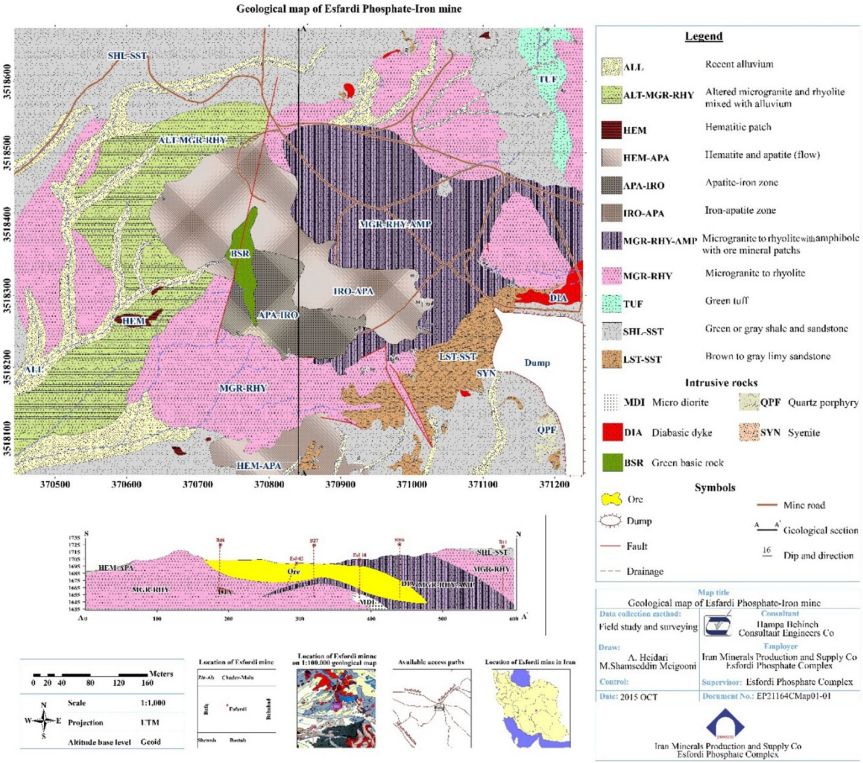

Figure 3. Geological map of the Esfordi phosphate deposit; scale 1:1,000

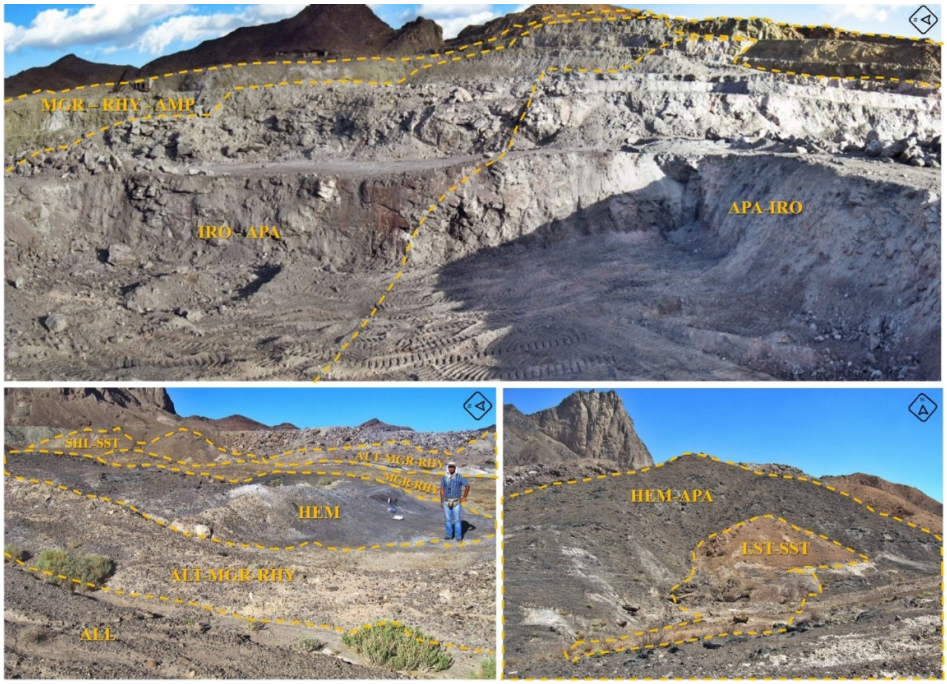

Figure 4. Images of outcrops of the rock units

Apatite-iron zone (APA-IRO): Best outcrops of this zone are in the southern part of the mine pit. The zone is a combination of apatite, hematite, magnetite, and tremolite- actinolite. Apatite mineralization in form of patches of different size is the characteristic feature of this zone.

Iron-apatite zone (IRO-APA): This zone has a considerable expansion in the northern part of the apatite-iron zone and in the north and northwest sections of the mine pit. The grade of iron and the amount of apatite in this zone decrease from north to northeast. The minerals that build up this zone are hematite, magnetite, apatite, and tremolite- actinolite. The less apatite content is the characteristic difference between this zone and the iron-apatite zone.

Amphibole-bearing rhyolite zone (RHY-AMP): This zone is developed in the peripheral parts of the ore, especially in the north of the mine pit. The rocks are mainly rhyolite to rhyolitic tuffs and contain considerable amounts of amphibole minerals. Ore minerals as patches, lenses, and scattered apatite and hematite veins, may be considerable in some parts of the zone.

Iron-apatite flow zone (HEM-APA): In the southwestern part of the mine, hematite and apatite are associated with significant surface exposure of thin lava flows, covering other rock and mineral assemblages. This unit is considered here as an iron-apatite immiscible liquid.

Hematite patches (HEM): The iron-rich hydrothermal solutions have caused a number of bodies, veins, and impregnations of hematite mineralization in the rocks. Some of these types of iron ores, which are more noticeable in the western part of the deposit, have significant economic volumes.

Discussion

Dataset

Sampling is the crucial source of information used in the geochemical and geological studies of ore deposits; studied area; thus, accurate sampling and sample preparation are important (Yasrebi, 2014). In this study, 41 samples were taken from different rock and mineral units inside and around the ore in order to investigate the anomaly status and the distribution of rare

earth elements (Figure 5).

The samples were analyzed by ICP-MS for a number of rare earth elements in the Iran Minerals Processing Research Center (IMPRC); each one is listed with its detection limit in Table 2. After preparing the "raw data", the data was processed in terms of censored values and replaced by the simple replacement method (Hawkes & Webb, 1979). Due to the large number of rare earth elements, the sum of these elements (∑REEs) was used.

Statistical and geostatistical analysis

To use the data more accurately and to analyse the results more appropriately, it was important to evaluate and identify the characteristics of the raw data used in the estimation. The results of the statistical analysis of the raw data are shown in Figure 6a. Clearly, the raw data has an abnormal distribution. Since it is necessary to use normal standard data for using SGS method, the normal standard transform operation was performed over the data, as shown in Figure 6b. The data had a variance and standard deviation of about 1 and a mean and skewness of about 0.

Table 2. Analyses of rare earth elements and their detection limits

Element (ppm)	Detection limit		Number of Censored values		Substitute values	
	Lower	Upper	Lower	Upper	Lower	Upper
Ce	1	6500	-	4	-	8667
Dy	5	120	9	9	3.75	160
Er	5	100	13	1	3.75	133.33
Eu	5	100	15	-	3.75	-
Gd	5	500	7	-	3.75	-
La	10	6500	1	-	7.5	-
Lu	3	100	41	-	-	-
Nd	1	6500	-	-	-	-
Pr	10	500	4	-	7.5	-
Sc	5	1000	33	-	-	-
Y	5	6500	1	-	3.75	-
Yb	5	40	15	6	3.75	53.33

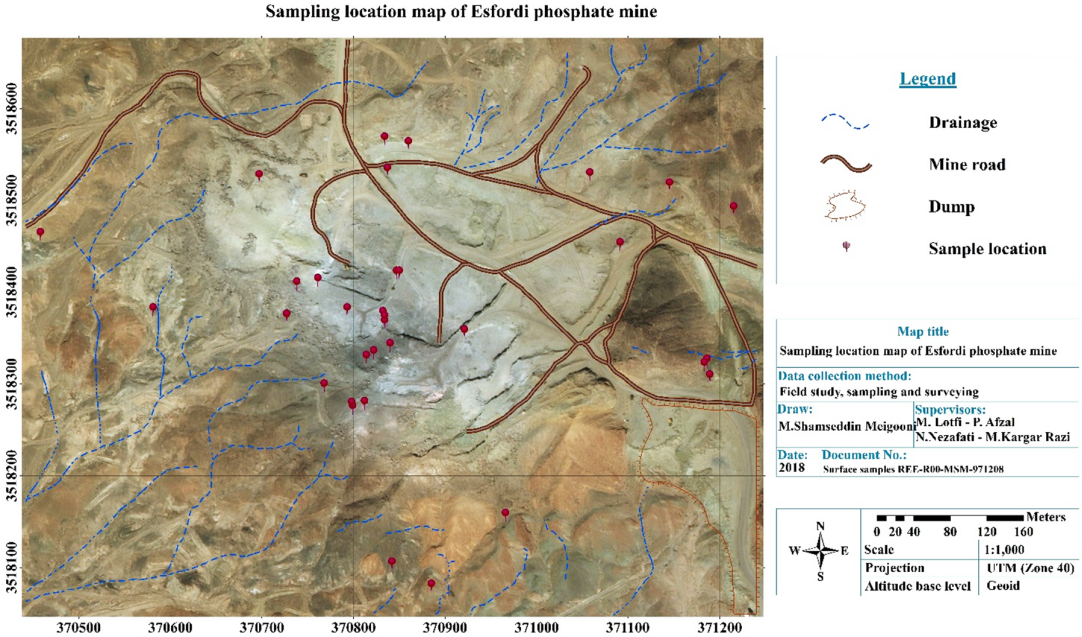

Figure 5. Samples' locations map within Esfordi deposit on satellite image

Variography is the most important tool for inferring and displaying spatial integration (David, 1970). It is used to analyze the status of the spatial structure of data, which is the basis of geostatistical estimations. After generating the standard normal data, the variogram was performed and an anisotropy ellipsoid was generated. The variogram and characteristics of the key parameters are shown in Figure 7.

Application of SGS

Providing an accurate geochemical anomaly map will be important and effective in providing efficient access to the ore mineral. To create various realizations via SGS, simulation was conducted 10 times by "ArcGIS 10.5" software based on standard normal data. The "simple kriging" method was used to estimate the cells. Kriging is the best unbiased linear geostatistical estimator which is capable of estimating both block and cell space (Journel, 1980; Machuca-Mory & Deutsch, 2009). For normal data, kriging ensures unbiased and minimal estimation variance (Webster & Oliver, 2007; Nas, 2009). In Gaussian simulation, each realization consists of random-specified value, it is possible to condition the simulation to increase the accuracy of the results. This process, which works with similar data used in estimation process ensures that the simulated values at each point adhere to the input data. Finally, the mean of both values is reported as the value of each cell (Journel, 1974).

In compliance with the sampling distance and the geological setting, each cell has a dimension of 10×10 m. After performing 10 simulation modes, statistical analysis was performed on the results of different realizations (Table 3). Finally, a unified map representing all realizations was created by calculating the average value of each cell ("E-Type") in 10 modes, and statistical studies were performed (Figure 8).

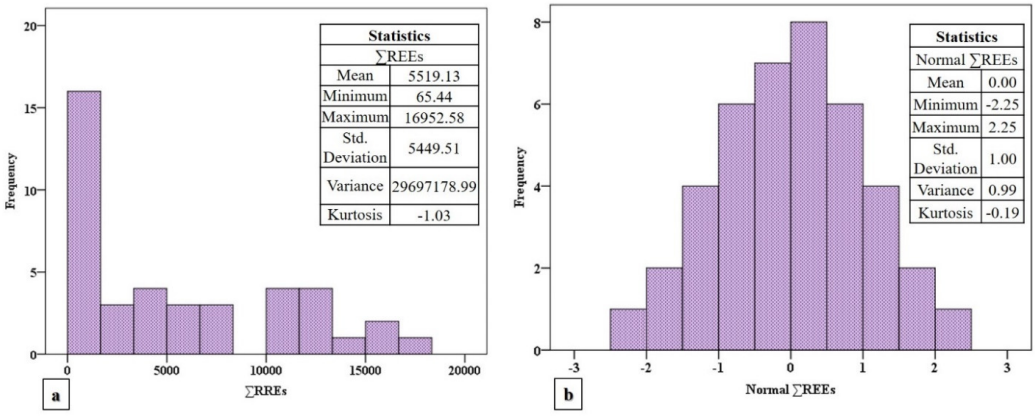

Figure 6. Histogram and statistical parameters: a, Raw data and b, Standardized normalized data

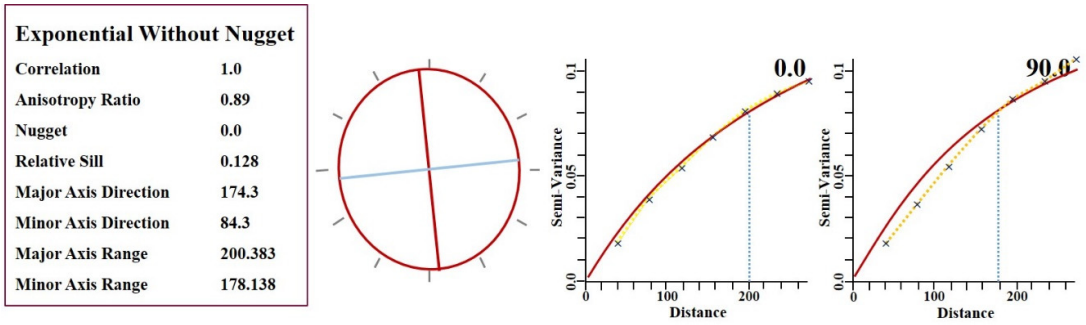

Figure 7. Variogram of the data and the best-fit model

Table 3. Statistical parameters of each realization obtained from the Gaussian simulation

Statistics ∑REEs (ppm)						
	Mean	Minimum	Maximum	Std. Deviation	Variance	Skewness
Realization1	4051.69	1.75	21629.20	3862.24	14916859.99	0.88
Realization2	4782.04	17.81	23905.50	4215.46	17770064.33	0.57
Realization3	3675.04	5.58	21993.90	3831.59	14681093.77	0.97
Realization4	3589.36	8.99	16656.00	3707.49	13745461.77	0.84
Realization5	4417.67	7.62	33367.30	4685.66	21955364.96	1.27
Realization6	3051.50	3.47	21391.80	3560.28	12675601.53	1.25
Realization7	3749.59	3.05	19879.50	3885.95	15100608.38	0.90
Realization8	4517.99	3.14	31671.30	5009.72	25097314.16	1.43
Realization9	3072.67	0.68	22932.30	3834.40	14702642.40	1.34
Realization10	3893.12	10.33	28190.60	3892.14	15148750.43	1.16

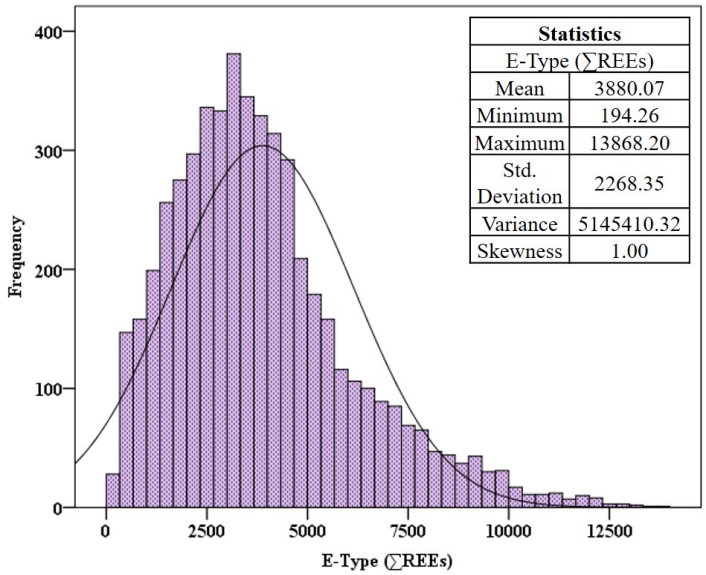

Figure 8. Histogram and statistical parameters of E-Type derived from data simulation

C-A fractal modeling

The calculation of high precision threshold values for anomalies and the separation of concentration communities are very important in construction of mineral potential maps (Yousefi et al., 2012; Shamseddin Meigoony et al., 2014). After the SGS simulation results were obtained, C-A fractal modeling was performed on the pixel values. The Log-Log plots and the threshold values for the four randomly selected realization modes (Realizations 1, 2, 5, and 6), and also the "E-Type" mode are shown in Figure 9.

After calculating the anomaly threshold, random selected maps and the E-Type map were plotted (Figures 10 and 11). As shown in the realization map (Figure 10), the main anomaly focus is in the central part of the deposit and corresponds to the extraction pit and its periphery.

It is clear from Figure 11 that the severe anomaly lies along the northeast-southwest approximation in the center of the mining area, which corresponds to the trend of the extraction pit. Comparison between this map and the geological map (Figure 3) clarifies that there is an association between the main anomalies with the apatite units and their marginal units existing in the studied area. Also, the existence of a fault with similar strike in the vicinity of the anomaly can confirm the result of the simulation method and the role of fault in mineral formation.

Thresholds of realization 1 and 7 ∑REEs (ppm)				
Low intensity	Moderate intensity	High intensity	Very high intensity	Extremely high intensity
199.5262	630.9573	5011.872	8317.638	12589.25

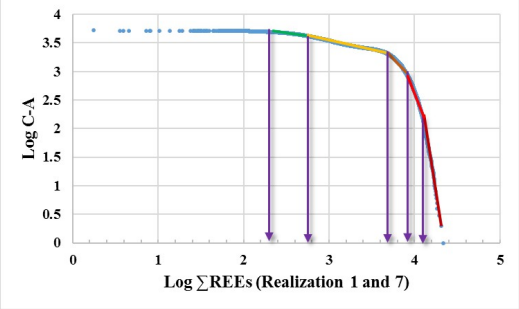

Thresholds of realization 2 and 4 ∑REEs (ppm)				
Low intensity	Moderate intensity	High intensity	Very high intensity	Extremely high intensity
158.4893	4786.301	7943.282	11220.18	15135.61

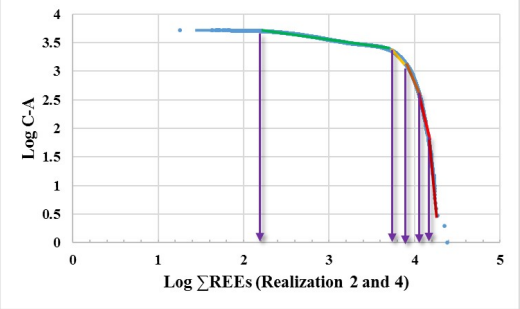

Thresholds of realization 3, 6, 9 and 10 ∑REEs (ppm)				
Low intensity	Moderate intensity	High intensity	Very high intensity	Extremely high intensity
199.5262	1445.44	4466.836	7079.458	12302.69

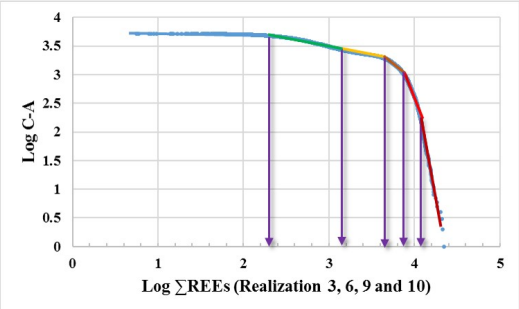

Thresholds of realization 5 and 8 ∑REEs (ppm)				
Low intensity	Moderate intensity	High intensity	Very high intensity	Extremely high intensity
158.4893	5011.872	7943.282	-	24547.09

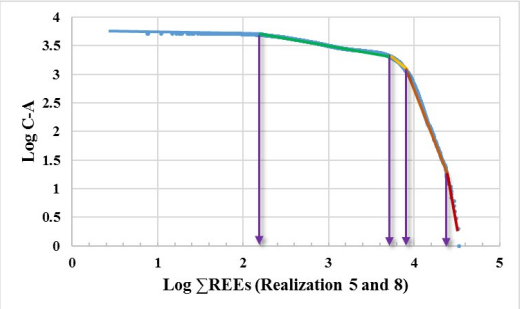

Thresholds of E-Type ∑REEs (ppm)				
Low intensity	Moderate intensity	High intensity	Very high intensity	Extremely high intensity
1096.478	3162.278	6456.542	9549.926	12302.69

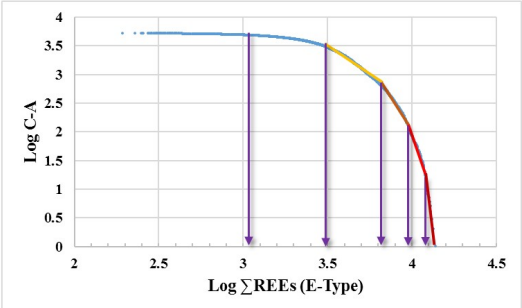

Figure 9. C-A fractal modeling log-log plot and specified threshold value

Application of log-ratio matrix

To better understand the ∑REE concentration distribution and to validate the SGS C-A fractal modeling maps, the correlation between different rock units of the mine and high concentration geochemical communities was investigated and overall accuracy (OA) was calculated.

This correlation between the concentration-rich communities identified by fractal modeling

(two stronger communities) and all existing rock units was assessed, and the main and indicative rock units associated with mineralization, including microgranite to rhyolite (MGR-RHY), amphibole-bearing microgranite to rhyolite, containing ore mineral patches (MGR-RHY-AMP), iron-apatite zone (IRO-APA), and apatite-iron zone (APA-IRO), are listed in the Table 4.

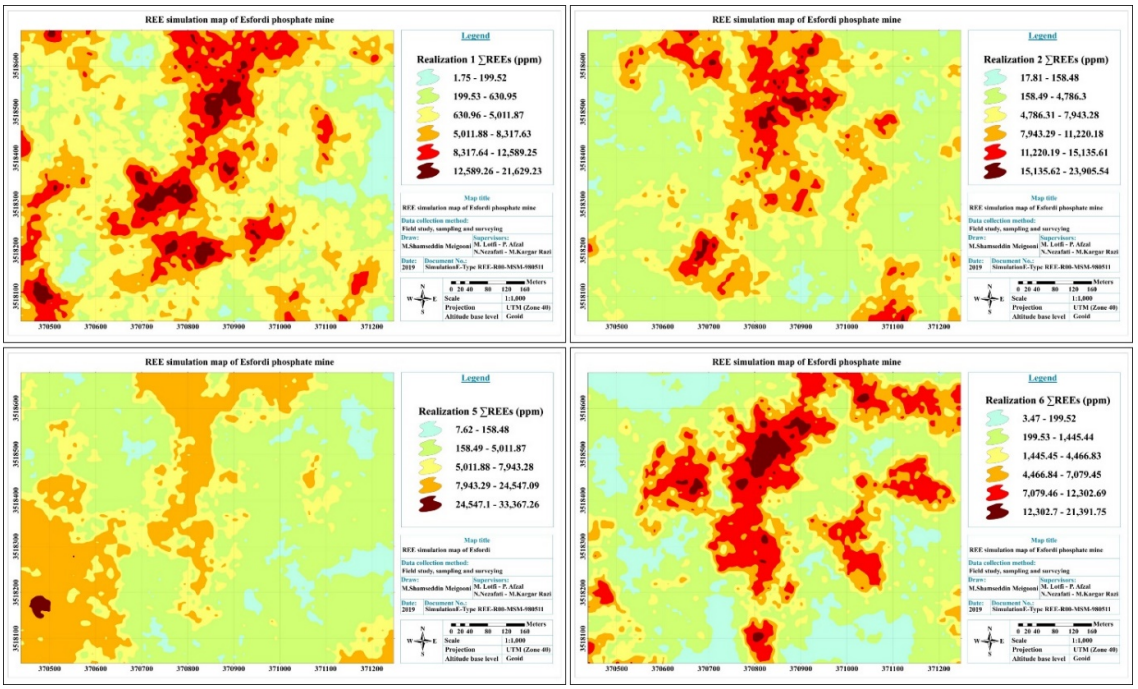

Figure 10. Random selected ∑REEs realizations obtained from the SGS simulation based on the C-A fractal modeling

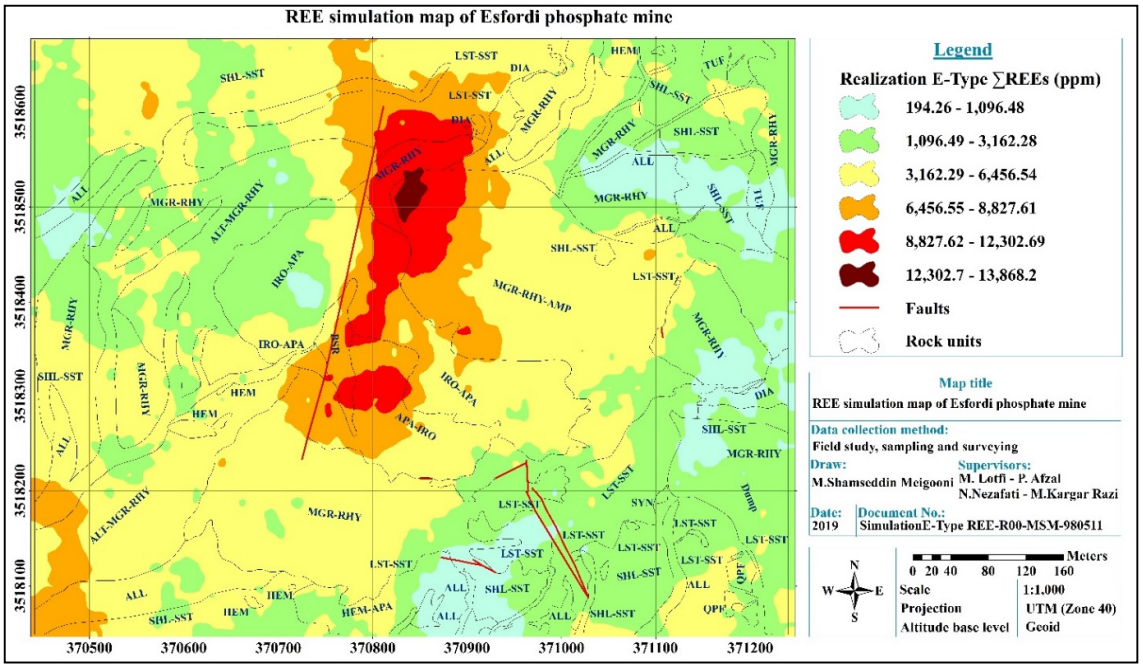

Figure 11. E-Type map of ∑REEs derived from the SGS simulation based on the C-A fractal modeling with faults and rock units (explanation of rock units based on Figure 3)

Based on the log-ratio matrix results (Table 4), it is clear that in all evaluated realizations as well as the E-type, the determined anomalies have strong correlation with APA-IRO, IRO-APA, MGR-RHY-AMP, and MGR-RHY and no significant correlation with other rock units in the mine. Among these realizations, realization 2 with OA = 0.89 has the greatest correlation with the APA-IRO unit. However, other realizations especially the E-Type, has similar OAs. It is important to note that all four units mentioned above have significant correlations with the specified anomalies containing apatite of various forms. As a result, this point can be considered as a guide for further exploration and investigation.

Table 4. Overall accuracy (OA) and T1E and T2E associated with concentration rich geochemical communities identified by SGS C-A fractal modeling and rock units

		MGR-RHY		**MGR-RHY-AMP**		**APA-IRO**		**IRO-APA**	
		Inside Zone	Outside Zone	Inside Zone	Outside Zone	Inside Zone	Outside Zone	Inside Zone	Outside Zone
Realization 1 ∑REE>8317.6 (ppm)	Inside Zone	A= 216	B= 594	A= 130	B= 680	A= 53	B= 575	A= 77	B= 733
	Outside Zone	C= 832	D= 3318	C= 508	D= 3642	C= 102	D= 4048	C= 325	D= 3825
		T1E= 0.79		T1E= 0.79		T1E= 0.65		T1E= 0.8	
		T2E= 0.15		T2E= 0.15		T2E= 0.15		T2E= 0.16	
		OA= 0.71		OA= 0.76		OA= 0.82		OA= 0.78	
Realization 2 ∑REE>11220.1 (ppm)	Inside Zone	A= 87	B= 315	A= 81	B= 321	A= 8	B= 394	A= 53	B= 349
	Outside Zone	C= 961	D= 3597	C= 557	D= 4001	C= 147	D= 4411	C= 349	D= 4209
		T1E= 0.91		T1E= 0.87		T1E= 0.94		T1E= 0.86	
		T2E= 0.08		T2E= 0.07		T2E= 0.08		T2E= 0.07	
		OA= 0.74		OA= 0.82		OA= 0.89		OA= 0.85	
Realization 5 ∑REE>7943.2 (ppm)	Inside Zone	A= 226	B= 962	A= 40	B= 1088	A= 54	B= 1074	A= 78	B= 1050
	Outside Zone	C= 822	D= 2950	C= 598	D= 3234	C= 101	D= 3731	C= 324	D= 3508
		T1E= 0.78		T1E= 0.93		T1E= 0.65		T1E= 0.8	
		T2E= 0.24		T2E= 0.25		T2E= 0.22		T2E= 0.23	
		OA= 0.64		OA= 0.66		OA= 0.76		OA= 0.72	
Realization 6 ∑REE>079.4 (ppm)	Inside Zone	A= 130	B= 689	A= 158	B= 661	A= 82	B= 737	A= 160	B= 659
	Outside Zone	C= 918	D= 3223	C= 480	D= 33661	C= 73	D= 4068	C= 242	D= 3899
		T1E= 0.87		T1E= 0.75		T1E= 0.47		T1E= 0.6	
		T2E= 0.17		T2E= 0.15		T2E= 0.15		T2E= 0.14	
		OA= 0.67		OA= 0.76		OA= 0.83		OA= 0.81	
E-Type ∑REE>8317.6 (ppm)	Inside Zone	A= 64	B= 618	A= 155	B= 527	A= 91	B= 591	A= 106	B= 576
	Outside Zone	C= 984	D= 3294	C= 483	D= 3795	C= 64	D= 4214	C= 296	D= 3982
		T1E= 0.93		T1E= 0.75		T1E= 0.41		T1E= 0.73	
		T2E= 0.15		T2E= 0.12		T2E= 0.12		T2E= 0.12	
		OA= 0.67		OA= 0.79		OA= 0.86		OA= 0.82	

Conclusion

In this study, the SGS simulation method was applied in order to adhere to data covariance models because of its computational efficiency and productivity in generating various realizations.

∑REE concentration investigation in the Esfordi deposit showed an average grade of 5519 ppm in samples and 3880 ppm in the E-Type map obtained from simulation. Fractal C-A modeling with five separated geochemical communities, yielded grades of 9549.92 ppm and 12302.69 ppm, which are regarded to be very high intensity and extremely high intensity thresholds, respectively.

The evaluation of the correlation and adoption of the E-Type map with rock units using log-ratio matrix indicate that geochemical anomalies with OA = 0.86 are best correlated with APA-IRO units. In addition, geochemical anomalies are well in association with other units such as IRO-APA, MGR-RHY-AMP, and MGR-RHY. This is indicative of correlation between REE concentrations and apatite mineralization. MGR-RHY-AMP unit (known as the "green rock" in the property), despite being identified in the anomalous community (due to containing apatite crystals), is transferred to the tailing dump. Therefore, reconsideration has to be conducted since there are volume of REEs and apatite crystals in the mine tailing dump.

In this research, the calculation and validation showed that the simultaneous application of geostatistical simulation and fractal modeling can be effective and useful in accurately identifying and separating anomalous communities.

Acknowledgments

The authors would like to thank the editor and two anonymous referees who kindly reviewed the earlier version of this manuscript and provided valuable suggestions and comments.

References

Afzal, P., Aramesh Asl, R., Adib, A., Yasrebi, A.B., 2015. Application of fractal modelling for Cu mineralisation reconnaissance by ASTER multispectral and stream sediment data in Khoshname area, NW Iran. Journal of the Indian Society of Remote Sensing 43(1): 121-132.

Afzal, P., Fadakar Alghalandis, Y., Khakzad, A., Moarefvand, P., Rashidnejad Omran, N., 2011. Delineation of mineralization zones in porphyry Cu deposits by fractal concentration–volume modeling. Journal of Geochemical Exploration 108(3): 220-232.

Afzal, P., Khakzad, A., Moarefvand, P., Rashidnejad Omran, N., Esfandiari, B., Fadakar Alghalandis, Y., 2010. Geochemical anomaly separation by multifractal modeling in Kahang (Gor Gor) porphyry system, Central Iran. Journal of Geochemical Exploration 104(1-2): 34-46.

Afzal, P., Mirzaei, M., Yousefi, M., Adib, A., Khalajmasoumi, M., Zia Zarifi, A., Foster, P., Yasrebi, A.B., 2016. Delineation of geochemical anomalies based on stream sediment data utilizing fractal modeling and staged factor analysis. Journal of African Earth Sciences 119: 139-149.

Afzal, P., Shahbeik, S., Moarefvand, P., Yasrebi, A.B., Zuo, R., Wetherelt, A., 2014. The Effect of Estimation Methods on Multifractal Modeling for Mineralized Zone Delineation in the Dardevey Iron Ore Deposit, NE Iran. Iranian Journal of Earth Sciences 6(1): 78-90.

Afzal, P., Yasrebi, A.B., Daneshvar Saein, L., Panahi, S., 2017. Prospecting of Ni mineralization based on geochemical exploration in Iran. Journal of Geochemical Exploration 181: 294-304.

Afzal, P., Yusefi, M., Mirzaie, M., Ghadiri-Sufi, E., Ghasemzadeh, S., Daneshvar Saein, L., 2019. Delineation of podiform-type chromite mineralization using geochemical mineralization prospectivity index and staged factor analysis in Balvard area (SE Iran). Journal of Mining and Environment 10(3): 705-715.

Afzal, P., Zia Zarifi, A., Farhadi Khankandi, S., Wetherelt, A., Yasrebi, B.A., 2012. Separation of uranium anomalies based on geophysical airborne analysis by using Concentration-Area (CA)

Fractal Model, Mahneshan 1: 50000 Sheet, NW IRAN. Journal of Mining and Metallurgy A: Mining 48(1): 1-11.

Agterberg, F., 1995. Multifractal modeling of the sizes and grades of giant and supergiant deposits. International Geology Review 37(1): 1-8.

Ahmadfaraj, M., Mirmohammadi, M., Afzal, P., Yasrebi, A.B., Carranza, E.J., 2019. Fractal modeling and fry analysis of the relationship between structures and Cu mineralization in Saveh region, Central Iran. Ore Geology Reviews 107: 172-185.

Asghari, O., Soltni, F., Bakhshandeh Amnieh, H., 2009. The comparison between sequential gaussian simulation (SGS) of Choghart ore deposit and geostatistical estimation through ordinary kriging. Australian Journal of Basic and Applied Sciences 3(1): 330-341.

Bonyadi, Z., Davidson, G.J., Mehrabi, B., Meffre, S., Ghazban, F., 2011. Significance of apatite REE depletion and monazite inclusions in the brecciated Se–Chahun iron oxide–apatite deposit, Bafq district, Iran: insights from paragenesis and geochemistry. Chemical Geology 281(3-4): 253-269.

Carranza, E.J.M., 2011. Analysis and mapping of geochemical anomalies using logratio-transformed stream sediment data with censored values. Journal of Geochemical Exploration 110(2): 167-185.

Carranza, E.J.M., 2017. Geochemical mineral exploration: should we use enrichment factors or log-ratios? Natural Resources Research 26(4): 411-428.

Carranza, E.J.M., Zuo, R., Cheng, Q., 2012. Fractal/multifractal modelling of geochemical exploration data. Journal of Geochemical Exploration 122: 1-3.

Chen, F., Chen, S., Peng, G. 2012. Using sequential gaussian simulation to assess geochemical anomaly areas of lead element. In: International Conference on Computer and Computing Technologies in Agriculture. Springer, 69-76.

Cheng, Q., Agterberg, F., Ballantyne, S., 1994. The separation of geochemical anomalies from background by fractal methods. Journal of Geochemical Exploration 51(2): 109-130.

Cheuiche Godoy, M., Dimitrakopoulos, R., Costa, J.F. 2001. Economic functions and geostatistical simulation applied to grade control. In: The Australasian Institute of Mining and Metallurgy, 591-599.

Daliran, F., 2002. Kiruna-type iron oxide-apatite ores and apatitites of the Bafq district, Iran, with an emphasis on the REE geochemistry of their apatites. Hydrothermal iron oxide copper gold and related deposits: a global perspective 2: 303-320.

Daneshvar Saein, L., Afzal, P., 2017. Correlation between Mo mineralization and faults using geostatistical and fractal modeling in porphyry deposits of Kerman Magmatic Belt, SE Iran. Journal of Geochemical Exploration 181: 333-343.

David, M., 1970. Geostatistical ore reserve estimation, Elsevier, Amsterdam, 1-283.

Davis, J.C., 2002. Statistics and data analysis in geology, John Wiley and Sons Inc., New York, 1- 638.

Deutsch, C., 2002. Goestatistical reservoir modeling, Oxford University Press, New York, 1-371.

Deutsch, C.V., Journel, A.G., 1992. Geostatistical software library and user's guide, Oxford University Press, New York, 1-340.

Dubrule, O., 2003. Geostatistics for seismic data integration in earth models, Society of Exploration Geophysicists and European Association of Geoscientists and Engineers, Oklahoma, 1-283.

Emery, X., Lantuéjoul, C., 2006. Tbsim: A computer program for conditional simulation of three-dimensional gaussian random fields via the turning bands method. Computers & Geosciences 32(10): 1615-1628.

Farahmandfar, Z., Jafari, M., Afzal, P., Ashja Ardalan, A., 2020. Description of gold and copper anomalies using fractal and stepwise factor analysis according to stream sediments in NW Iran. Geopersia 10(1): 135-148.

Foerster, H., Jafarzadeh, A., 1994. The Bafq mining district in central Iran; a highly mineralized Infracambrian volcanic field. Economic Geology 89(8): 1697-1721.

Gholampour, O., Hezarkhani, A., Maghsoudi, A., Mousavi, M., 2019. Delineation of alteration zones based on kriging, artificial neural networks, and concentration–volume fractal modelings in hypogene zone of Miduk porphyry copper deposit, SE Iran. Journal of Mining and Environment 10(3): 575-595.

Goncalves, M.A., Mateus, A., Oliveira, V., 2001. Geochemical anomaly separation by multifractal modelling. Journal of Geochemical Exploration 72(2): 91-114.

Goovaerts, P., 1997. Geostatistics for natural resources evaluation, Oxford University Press, New York,

1-483.
Goovaerts, P., 2008. Kriging and semivariogram deconvolution in the presence of irregular geographical units. Mathematical Geosciences 40(1): 101-128.
Haghipour, A., 1964. Iron ore deposits in Central Iran, in relation to structural geology and metamorphism, scapolitization and albitization. Journal of Iranian Petroleum Institute 76: 1-9.
Hajsadeghi, S., Asghari, O., Mirmohammadi, M., Afzal, P., Meshkani, S.A., 2017. Uncertainty-Volume fractal model for delineating copper mineralization controllers using geostatistical simulation in Nohkouhi volcanogenic massive sulfide deposit, Central Iran. Maden Tetkik ve Arama Dergisi (159): 1-10.
Hassanpour, S., Afzal, P., 2013. Application of concentration–number (C–N) multifractal modeling for geochemical anomaly separation in Haftcheshmeh porphyry system, NW Iran. Arabian Journal of Geosciences 6(3): 957-970.
Hawkes, H.E., Webb, J.S., 1979. Geochemistry in mineral exploration, Academic Press, New York, 1-657.
Jami, M. 2006. Geology, geochemistry and evolution of the Esfordi phosphate-iron deposit, Bafq area, Central Iran. In: University of New South Wales, Australia.
Jami, M., Dunlop, A.C., Cohen, D.R., 2007. Fluid inclusion and stable isotope study of the Esfordi apatite-magnetite deposit, Central Iran. Economic Geology 102(6): 1111-1128.
Jebeli, M., Afzal, P., Pourkermani, M., Jafari Rad, A., 2018. Correlation between rock types and Copper mineralization using fractal modeling in Kushk-e-Bahram deposit, Central Iran. Geopersia 8(1): 131-141.
Journel, A., 1980. The lognormal approach to predicting local distributions of selective mining unit grades. Journal of the International Association for Mathematical Geology 12(4): 285-303.
Journel, A.G., 1974. Geostatistics for conditional simulation of ore bodies. Economic Geology 69(5): 673-687.
Journel, A.G., Huijbregts, C.J., 1978. Mining geostatistics, Academic press, London, 1-600.
Kühn, C., Visser, J.K., 2014. Managing uncertainty in typical mining project studies. South African Journal of Industrial Engineering 25(2): 105-120.
Machuca-Mory, D.F., Deutsch, C.V., 2009. Sequential Gaussian and Indicator Simulation with Location-Dependent Distributions and Statistics. Centre for Computational Geostatistics 11.
Madani Esfahani, N., Asghari, O., 2013. Fault detection in 3D by sequential Gaussian simulation of Rock Quality Designation (RQD). Arabian Journal of Geosciences 6(10): 3737-3747.
Manchuk, J.G. 2010. Geostatistical modeling of unstructured grids for flow simulation. In: University of Alberta, Canada.
Mandelbrot, B.B., 1983. The fractal geometry of nature, WH freeman, New York, 1-468.
Mokhtari, M.A.A., 2015. Posht-e-Badam metallogenic block (central Iran): A suitable zone for REE mineralization. Central European Geology 58(3): 199-216.
Nas, B., 2009. Geostatistical Approach to Assessment of Spatial Distribution of Groundwater Quality. Polish Journal of Environmental Studies 18(6): 1073–1082.
Navidi, A., Ziaii, M., Afzal, P., Yasrebi, A.B., Wetherelt, A., Foster, P., 2014. Determination of chromites prospects using multifractal models and zonality index in the parang 1: 100000 sheet, Iran. Universal Journal of Geoscience 2(4): 133-139.
Nazarpour, A., Sadeghi, B., Sadeghi, M., 2015. Application of fractal models to characterization and evaluation of vertical distribution of geochemical data in Zarshuran gold deposit, NW Iran. Journal of Geochemical Exploration 148: 60-70.
Pardo-Igúzquiza, E., Atkinson, P.M., 2007. Modelling the semivariograms and cross-semivariograms required in downscaling cokriging by numerical convolution–deconvolution. Computers & Geosciences 33(10): 1273-1284.
Queiroz, J.C.B., Sturaro, J.R., Riedel, P.S. 2001. Geostatistic Mapping of Arsenic, Manganese and Iron Contamination Risk in the Port of Santana, Amapa, Brazil. In: Annual Conf. of Int. Association for Mathematical Geology. Cancun, Mexico.
Rezaie, M., Afzal, P., 2016. The effect of estimation methods on fractal modelling for anomales' detection in the Irankuh area, Central Iran. Geopersia 6(1): 105-116.
Shahsavar, S., Jafari Rad, A., Afzal, P., Nezafati, N., 2020. Selection of Optimum Fractal Model for Detection of Stream Sediments Anomalies. Geopersia, 10.22059/GEOPE.2020.293961.648516.

Shamseddin Meigoony, M., Afzal, P., Gholinejad, M., Yasrebi, A.B., Sadeghi, B., 2014. Delineation of geochemical anomalies using factor analysis and multifractal modeling based on stream sediments data in Sarajeh 1: 100,000 sheet, Central Iran. Arabian Journal of Geosciences 7(12): 5333-5343.

Soltani, F., Afzal, P., Asghari, O., 2014. Delineation of alteration zones based on Sequential Gaussian Simulation and concentration–volume fractal modeling in the hypogene zone of Sungun copper deposit, NW Iran. Journal of Geochemical Exploration 140: 64-76.

Stosch, H.-G., Romer, R.L., Daliran, F., Rhede, D., 2011. Uranium–lead ages of apatite from iron oxide ores of the Bafq District, East-Central Iran. Mineralium Deposita 46(1): 9-21.

Taghipour, S., Kananian, A., Mackizadeh, M.A., K Somarin, A., 2015. Skarn mineral assemblages in the Esfordi iron oxide–apatite deposit, Bafq district, Central Iran. Arabian Journal of Geosciences 8(5): 2967-2981.

Torab, F., Lehmann, B., 2007. Magnetite-apatite deposits of the Bafq district, Central Iran: apatite geochemistry and monazite geochronology. Mineralogical Magazine 71(3): 347-363.

Torab, F.M. 2008. Geochemistry and metallogeny of magnetite apatite deposits of the Bafq mining district, Central Iran. In: Clausthal University of Technology, Germany.

Wang, X.-q., 2003. Exploration geochemistry: Past achievements and future challenges. Earth Science Frontiers 10(1): 239-248.

Webster, R., Oliver, M.A., 2007. Geostatistics for environmental scientists, John Wiley & Sons, New York, 1-270.

Yasrebi, A.B. 2014. Determination of an Ultimate Pit Limit Utilising Fractal Modelling to Optimise NPV. In: University of Exeter, Exeter, UK.

Yasrebi, A.B., Hezarkhani, A., 2019. Resources classification using fractal modelling in Eastern Kahang Cu-Mo porphyry deposit, Central Iran. Iranian Journal of Earth Sciences 11(1): 56-67.

Yousefi, M., Kamkar-Rouhani, A., Carranza, E.J.M., 2012. Geochemical mineralization probability index (GMPI): a new approach to generate enhanced stream sediment geochemical evidential map for increasing probability of success in mineral potential mapping. Journal of Geochemical Exploration 115: 24-35.

Zuo, R., 2011a. Decomposing of mixed pattern of arsenic using fractal model in Gangdese belt, Tibet, China. Applied Geochemistry 26: 271-273.

Zuo, R., 2011b. Identifying geochemical anomalies associated with Cu and Pb–Zn skarn mineralization using principal component analysis and spectrum–area fractal modeling in the Gangdese Belt, Tibet (China). Journal of Geochemical Exploration 111(1-2): 13-22.

Zuo, R., Cheng, Q., Xia, Q., 2009. Application of fractal models to characterization of vertical distribution of geochemical element concentration. Journal of Geochemical Exploration 102(1): 37-43.

Zuo, R., Wang, J., 2016. Fractal/multifractal modeling of geochemical data: A review. Journal of Geochemical Exploration 164: 33-41.

Zuo, R., Xia, Q., 2009. Application fractal and multifractal methods to mapping prospectivity for metamorphosed sedimentary iron deposits using stream sediment geochemical data in eastern Hebei province, China. Geochimica et Cosmochimica Acta 73: A1540.